Metallomics

Accepted Manuscript

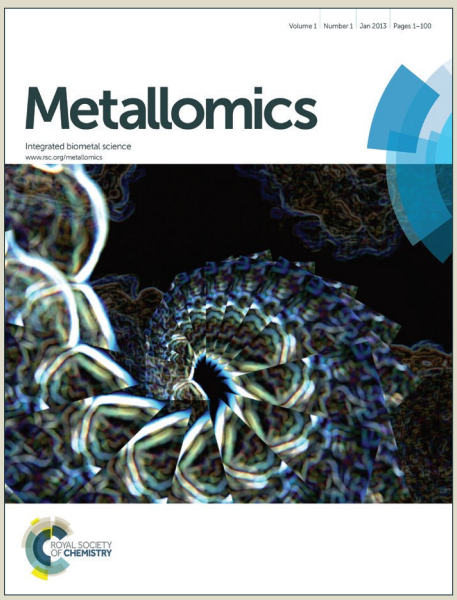

ROYAL SOCIETY OF CHEMISTRY

www.rsc.org/metallomics

Differential effects of metal ions on TCDD-induced cytotoxicity and cytochrome P4501A1 gene expression in a zebrafish liver (ZFL) cell-line

Ying Ying Chen and King Ming Chan[1]
School of Life Sciences, Chinese University, Sha Tin, Hong Kong SAR, China
[1] Corresponding author (Email: kingchan@cuhk.edu.hk)

Abstract

Trace metal ions and trace organic compounds are common co-contaminants in the environment that pose risks to human health. We evaluated the effects of four metal ions (As^{3+}, Cu^{2+}, Hg^{2+}, and Zn^{2+}) on 2,3,7,8-Tetrachlorodibenzo-p-Dioxin (TCDD) induced cytotoxicity and the expression of the cytochrome P4501A1 gene (*cyp1a1*) in the zebrafish liver (ZFL) cell line. A metal accumulation study showed that Cu and Zn did not accumulate in ZFL cells. However, As and Hg did accumulate, which resulted in the inhibition of TCDD-mediated induction of *cyp1a1* mRNA and protein expression, and 7-ethoxyresorufin O-deethylase activity. A luciferase assay showed that both As^{3+} and Hg^{2+} inhibited the TCDD-induced activity of gene constructs containing either synthetic 3XRE or a distal *cyp1a1* promoter region, implying that the decreased levels of TCDD-induced *cyp1a1* were due to transcriptional effects. A proteomic study showed that the toxic effects of As^{3+} might be due to changes in cellular metabolic processes, the cellular stimulation response and the cellular redox state in ZFL cells.

Keywords: biomarkers, combined effects, proteomics, trace metals

Introduction

The aromatic hydrocarbon receptor (AHR) plays a central role in the toxicity of numerous polycyclic aromatic hydrocarbons (PAHs), by controlling the expression of a battery of detoxification enzymes responsible for drug metabolism[1]. Cytochrome P4501A1 (CYP1A1) is an important AHR target gene, which is a phase I drug-metabolizing enzyme and useful biomarker for analyzing the cellular responses and actions of PAHs such as 2,3,7,8-Tetrachlorodibenzo-p-dioxin (TCDD), in both mammals and fish[22, 3]. The transcriptional activation of the *cyp1a1* gene is mediated by the binding of aromatic (or aryl) hydrocarbon (AH) ligands, such as TCDD or benzo(a)pyrene, to the cytosolic AHR. Upon ligand binding, the ligand–receptor complex dissociates from the heat shock protein HSP90 and migrates to the nucleus with the aryl hydrocarbon receptor nuclear translocator (ARNT)[4]. The entire complex then acts as a transcription factor that binds to xenobiotic responsive elements (XREs) located in the promoter region of the *cyp1a1* gene to activate its transcription[5].

In zebrafish, there are several isoforms of CYP1, AHR, and ARNT proteins. Five *cyp1* genes have been identified in this species: *cyp1a1, cyp1b1, cyp1c1, cyp1c2,* and *cyp1d1*[6]. Of these, *cyp1a1* is the most well studied and sensitive to PAH induction[6, 7]. Zebrafish possess three *ahr* genes: *ahr1a, ahr1b* and *ahr2*. Only AHR1B and AHR2 proteins are capable of binding to TCDD with high-affinity and are transcriptionally active[8, 9,10]. The induction of *cyp1* genes

in zebrafish is largely via AHR2[7, 11]. Experimental evidence has demonstrated that one form of ARNT2, ARNT2b, forms a functional heterodimer with AHR2 to induce XRE (xenobiotic response element) driven transcription following TCDD treatment[9, 12, 13]. Therefore, in this study we examined the expression of *cyp1a1, ahr2* and *arnat2b* in ZFL cells following the administration of metal ions and TCDD.

Among the various reactions catalyzed by CYP1A1, hydroxylation at an aromatic ring's vacant position is considered the hallmark of the initiation of carcinogenesis through the formation of highly reactive conversion products (such as epoxides) that can cause oncogenic mutations in experimental animals and humans[14] and other toxic effects including birth defects, immune suppression, and endocrine disruption[15].

Trace metals are highly toxic environmental contaminants that are not biodegradable[16]. Mercury and arsenic are two of the most toxic metal ions to humans[17]. Although some trace metals (such as copper and zinc) are essential to metabolism in the human body, they can lead to acute or chronic poisoning at higher concentrations. Exposure to trace metals comes from numerous sources, including air, water, soil, and food contaminated by industrial pollution, which can result in adverse effects on human metabolism. Trace metals and other environmental pollutants including classes of highly toxic and persistent environmental carcinogens such as PAHs (typified by TCDD), are common co-contaminants from hazardous waste treatment sites, such as electronic

waste dumps and thermal treatment facilities. These pollutants are also co-released from activities such as fossil fuel combustion and municipal waste incineration[18].

Previous studies have indicated that co-contamination by trace metals and PAHs could enhance or reduce the carcinogenicity of PAHs by modifying the expression of the *cyp1a1* gene[19, 20]. Recently, we observed that cadmium can inhibit CYP1A1 induction in ZFL cells (unpublished data). Although the regulation of CYP1A1 by trace metal ions has been documented in several cell lines and species, the currently available studies on the mechanisms of the regulation of different metals on CYP1A1 induction are controversial. Emerging evidence suggests that AHR ligand and metal co-treatment generates different biological responses than would be expected according to the toxicological mechanisms of each considered separately[21]. Any influence of metals on the capacity of AHR ligands to induce CYP1A1 will influence the carcinogenicity and mutagenicity of the AHR ligands. Therefore, there is a need to understand the mechanisms driving these responses and to define the exact role of AHR ligands and metals in the promotion of carcinogenesis.

Zebrafish is a useful model for studying developmental genetics and toxicology due to their rapid development, conserved molecular pathways and potential for high throughput screening[22]. Because the liver is the primary organ for metabolism, detoxification and homeostasis, understanding the molecular mechanisms involved in the modulation of AHR-related gene

expression by Cd^{2+} in a zebrafish liver (ZFL) cell line is useful and informative [23, 24].

As a first step to establishing the interaction between trace metals and AHR ligands, we undertook extensive studies to determine the effect of non-essential trace metals (Hg^{2+} and As^{3+}) and essential trace metals (Cu^{2+} and Zn^{2+}) on the induction of *cyp1a1* by TCDD in ZFL cells. Inhibition of *cyp1a1* gene expression was observed after exposure to non-essential metals but not essential metals. To further understand the inhibition mechanism of the non-essential metals on *cyp1a1,* two-dimensional electrophoresis (2-DE) and matrix-assisted laser desorption/ionization time-of-flight (MALDI-TOF) MS/MS approaches were also applied to elucidate the potential mechanism of As^{3+} on *cyp1a1* inhibition.

Toxicoproteomics is a relatively new discipline that applies global proteomic technologies to toxicological studies. Its aim is to detect critical proteins and pathways disrupted by exposure to harmful chemicals and environmental stressors[25]. It is also a powerful tool to reveal how trace metals affect *cyp1a1* expression and consequently alter CYP1A1 activity.

2. Materials and methods

2.1 Cell cultures and treatments

The ZFL cell line, obtained from the American Type Culture Collection (ATCC, CRL2643), was maintained in a standard culture medium comprising

50% L15 medium, 35% Dulbecco's modified medium (DMEM) and 15% Hams F12, supplemented with 1.5 g/L sodium bicarbonate, 15 mM HEPES, 0.01 mg/ml insulin, 50 ng/ml EGF, 5% heat-inactivated fetal bovine serum and a 1% penicillin/streptomycin mixture at 28°C, as previously described [23]. All of the reagents were purchased from GIBCO Invitrogen Cell Technologies, Life Technologies (NY, USA).

For the cellular treatments, the ZFL cells were seeded in 6-, 24- and 96-well cell culture plates and 100-mm cell culture dishes at an appropriate density in complete standard culture medium. A concentrated stock solution of 50 ppm TCDD (Cambridge Isotope Laboratories, MA, USA) in dimethyl sulfoxide (DMSO, cell culture grade, Steinheim, Germany) and 50 mM $CuCl_2$, 50 mM $ZnCl_2$, 10 mM $HgCl_2$ and 10 mM $AsCl_3$ (Sigma-Aldrich, St. Louis, USA) dissolved in double deionized water was prepared separately. The cells were treated in serum-free media with TCDD (3/30 nM) and/or a series of concentrations of Cu^{2+}, Zn^{2+}, Hg^{2+}, and As^{3+} (5%, 10%, or 25% LC50 values). The LC50s of Cu^{2+}, Zn^{2+}, Hg^{2+}, and As^{3+} on ZFL cells are 308.1 μM, 343.5 μM, 68.6 μM, and 44.3 μM respectively, as reported previously [26].

2.2 Cytotoxicity assay

Cytotoxicity assays were determined with AlamarBlue™ assays as previously described[27]. The ZFL cells were seeded on 96-well plates with a density of 1×10^5 per well and pre-incubated in the standard culture medium

overnight before exposure. After pre-incubation, the medium was removed and the cells were exposed to media with TCDD (3/30 nM) and/or a series of concentrations of Cu^{2+}, Zn^{2+}, Hg^{2+}, and As^{3+} (5%, 10%, or 25% LC50) for 24 h. Six replicates were performed on the same plate for each dose. The medium with TCDD and trace metals was replaced with 100 µL fresh medium containing 10% AlamarBlue™ (Biosource, Invitrogen, NY, USA) and incubated for 2 h. The fluorescent signal was measured using a fluorescent microplate reader (Polarion, TECAN, Switzerland) with an excitation wavelength of 535 nm and an emission wavelength of 595 nm. The percentage of cytotoxicity was calculated by rating the control and treatment group readings.

2.3 Determination of metal concentrations in zebrafish and ZFL cells

The ZFL cells were exposed to a series of concentrations of Cu^{2+}, Zn^{2+}, Hg^{2+}, and As^{3+} (5%, 10%, or 25% of the LC50 values) with or without 3 nM TCDD. All samples were harvested, weighed, and digested with concentrated nitric acid (Merck) at 60 °C for 4 h. Concentrations of Cu and Zn were determined with graphite furnace atomic absorption spectrophotometry (Hitachi Z2700)[21], and concentrations of Hg and As were determined with flame atomic absorption spectrophotometry (Hitachi Z2300). The results are expressed as mg metal/kg cells. Each treatment was performed in triplicate.

2.4 Determination of enzyme activity

The CYP1A1-dependent 7-ethoxyresorufin O-deethylase (EROD) activity in intact, living cells was assessed using 7-ethoxyresorufin (7-ER, Sigma-Aldrich, St. Louis, USA) as a substrate, following a previous method[28] with some optimization. The ZFL cells were seeded into 96-well plates, 10^5 cells per well. The next day, the medium was replaced with freshly made medium containing a series of concentrations of Cu^{2+}, Zn^{2+}, Hg^{2+}, and As^{3+} (5%, 10%, or 25% LC50) and TCDD. After incubation for 24 h, the cells were rinsed twice with ice-cold Tris-HCl (pH 7.4) and then pre-incubated with 5 μM of 7-ethoxyresorufin (7-ER), 80 ul per well, at 28 °C with shaking. After 20 min, 5 mM of NADPH (Sigma-Aldrich, St. Louis, USA), 20 ul per well, was added to initiate the EROD reaction. After 10 min, the reaction was stopped using ice-cold methanol. The EROD activity in the wells was analyzed by measuring resorufin production fluorometrically (530 nm excitation and 590 nm emission) using a fluorescent plate reader (Polarion, TECAN, Switzerland). Then the protein concentration of each well was measured for calibration.

2.5 Protein extraction and Western blot analysis

After incubation with Cu^{2+}, Zn^{2+}, Hg^{2+}, As^{3+} and TCDD as described above, the ZFL cells were collected in an RAPI lysis buffer (25 mM Tris-HCl (pH 7.6), 150 mM NaCl, 1% NP-40, 1% sodium deoxycholate, 0.1% SDS) and 10 μl/ml of 100× protease inhibitor (Thermo Fisher Scientific, MA, USA)[22]. The total cellular proteins were obtained by incubating the cell lysates on ice for 30 h,

with intermittent homogenization every 10 min, followed by centrifugation at 12,000× *g* for 30 min at 4 °C. The supernatant fractions were collected to determine the protein concentration using a BCA protein assay kit (Pierce, Thermo Fisher Scientific, MA, USA). Western blot analyses were performed using a previously described method. Briefly, 30 μg of protein from each treatment group was separated by 10% sodium dodecyl sulfate (SDS)-polyacrylamide gel, and then electrophoretically transferred to polyvinylidene difluoride membranes. Protein blots were then blocked overnight at 4 °C in TBST (50 mM Tris-base, 0.15 M sodium chloride, 0.1% Tween-20) containing 5% skim milk powder. After blocking, the blots were incubated for 2 h at room temperature with a primary polyclonal anti-rabbit CYP1A1 antibody (GeneTex, Hsinchu City, Taiwan, Republic of China, 1:800) in TBST solution. The membranes were washed three times with TBST and incubated for 1 h with a secondary antibody, HRP-conjugated goat anti-rabbit IgG (Pierce, Thermo Fisher Scientific, MA, USA, 1:5000). The membranes were then washed three more times and the bands were visualized using the enhanced chemiluminescence method according to the manufacturer's instructions (Santa-Cruz Biotechnology, Texas, USA).

2.6 RNA extraction, cDNA synthesis and real-time polymerase chain reaction

Samples of zebrafish liver cells, embryos, larvae, and organs exposed to a

series of concentrations of Cu^{2+}, Zn^{2+}, Hg^{2+}, As^{3+} and TCDD as described above, were collected for total RNA extraction using the Trizol reagent (Takara Biotechnology, Japan). Reverse transcriptions (RTs) were performed using the PrimerScript™ RT reagent kit (Takara Biotechnology, Japan) according to the manufacturer's instructions. A 1 μg RNA template from each sample was then converted into cDNA in a 20 μl volume at 42 °C for 30 min. The reverse transcription products were quantified using NANODROP 2000C (Thermo Fisher Scientific, MA, USA).

The mRNA expression changes in the AHR pathway-related genes in the ZFL cells and zebrafish exposed to different concentrations of Cd^{2+} and TCDD were verified with real-time quantitative polymerase chain reaction (PCR) methods using the ABI 7500 Fast system (Applied Biosystems, CA, USA). The glyceraldehyde 3-phosphate dehydrogenase (GAPDH) was the most stable reference gene after exposure to Cd^{2+} and TCDD, and thus was used as the internal control for normalization[23]. SYBR® Green PCR Master Mix (Takara Biotechnology, Japan) was used in the real-time PCR analysis. All of the gene sequences used in this study were obtained from the NCBI Gene Bank and the latest zebrafish genome databases (Zv9 and Vega49). The primer sets were designed using the NCBI PCR Primer Design online tool, Primer-BLAST (http://www.ncbi.nlm.nih.gov/tools/primer-blast). The nucleotide sequences of the forward and reverse primers for the genes selected and their accession numbers are listed in Table 1 and validated as described in Chen et al.

(2014)[23]. The relative expression of each gene was calculated as previously described using the formula of relative fluorescence = $2^{\Delta\Delta Ct}$.

2.7 Transient gene expression study and luciferase assay

The ZFL cells were maintained according to the methods described in section 2.1. The cells were seeded in 24-well plates and incubated for 24 h before transfection. A reporter vector was introduced into cells using Lipofectamine 2000 reagent (Life Technologies, Inc., Carlsbad, USA) following the manufacturer's protocols. Triplicated transfections were performed using 500 ng of total DNA containing 400 ng reporter vector and 100 ng pRL-TK vector (Promega, Madison, USA) as internal controls. After transfection, the cells were exposed to different concentrations of Cu^{2+}, Zn^{2+}, Hg^{2+}, As^{3+} and TCDD for 24 h. The cells were then harvested to determine luciferase activity using the Dual-Luciferase® Reporter Assay System (Promega, Madison, USA), according to the manufacturer's instructions, with a GloMax-96-Micro plate Luminometer (Promega, Madison, USA). The data were analyzed using one-way ANOVA with GraphPad Prism® 5 software.

2.8 Isolation of the cytosolic fraction

The treated ZFL cells were thawed at room temperature and suspended in a 200 µl native lysis buffer I (25 mM Tris–HCl, 2 mM DTT, 20 µM PMSF, pH 7.4)[22]. The cells were then lysed by ultrasonic fragmentation at 4 °C for 10 min.

The sample was then centrifuged at 1500 × *g* for 10 min. The supernatant was further centrifuged at 105,000 × *g* for 30 min to collect the cytosolic fraction. All centrifugations were processed at 4 °C. Then the supernatant was collected and purified by 2D-Clean KIT (Sigma-Aldrich, St. Louis, USA) and the pellet was resolved in lysis buffer II (8 M urea, 4% CHAPS, 2 M thiourea, 50 mM DTT, 10 mM Tris, 1 mM EDTA, and 0.0002% bromophenol blue). The protein concentration was determined using the Bradford protein assay (Bio-Rad, USA) with bovine serum albumin as the standard, then each sample was adjusted to 2 mg/ml and aliquots were stored at −80 °C.

2.9. Two-dimensional gel electrophoresis (2-DE) and in-gel digestion and protein identification

Two-dimensional gel electrophoresis (2-DE) and in-gel digestion and protein identification were performed according to previously reported procedures[22,29]. Briefly, the cytosolic samples were mixed with a rehydration buffer and then isoelectric focusing (IEF) was carried out using Ettan IPGphor (GE Health, USA) with precast immobilized pH gradient (IPG) strips (ready-strip IPG strips, pH range 3–10, 13 cm long, GE Health, USA). A total of 350 μg protein was loaded and incubated for 12 h at 20 °C with 30 V, followed by IEF for 2 h with 500 V, 1 h with 1000 V, the gradient elevating to 8000 V for 25,000 Vh and 8000 V continued for 10,000 Vh. After the IEF steps, the IPG strips were incubated at room temperature for 15 min in an equilibration buffer, and a

second equilibration step was carried out for another 15 min under the same conditions, except that the dithiothreitol was replaced with 135 mM iodoacetamide. The equilibrated strips were then loaded onto 12% polyacrylamide (14 cm × 16 cm, 1 mm thick) with SDS and a 2 cm stacking gel of 4% polyacrylamide placed on top. After separation, the proteins were visualized by silver staining, as recommended by the manufacturer (GE Health, USA), and each treatment was replicated three times. The 2-DE images were scanned and analyzed using ImageMaster 2-D Elite software. Image spots were initially automatically outlined and matched, and then manually edited. The intensity volume of each spot was calculated by background subtraction and total spot volume normalization, and the resulting spot volume percentage was used for comparison. For each treatment, three 2-DE gels were used for analysis, and those spots with more than 1.2 fold difference were picked up for identification.

The protein spots of interest were manually excised from the 2-DE gels. Each protein sample was further processed by enzymatic digestion with trypsin to generate peptide fragments. The tryptic peptides were mixed with 4 mg/ml acyano-4-hydroxycinnamic acid (CHCA) in 50% ACN and 0.1% TFA, spotted onto the target plate and allowed to dry. MALDI–TOF MS was performed with a Bruker Ultrflextreme MALDI-TOF/TOF spectrometer (Bruker Daltonik GmbH, Bremen, Germany). Mass data acquisitions were piloted by FlexControl software using the automatic run. All MS survey scans were acquired over the

mass range 500–4000 m/z in the reflectron positive-ion mode and accumulated from 4000 laser shots with acceleration of 20 kV. The data were searched by ProteinScape 3.0 using MASCOT (Matrix Sciences, London, United Kingdom) as a search engine against the NCBI database or Swiss protein database.

2.10 Bioinformatic analysis of 2-DE data

The differentially expressed proteins were subjected to PANTHER 10.0 classification (www.pantherdb.org)[30] and DAVID[31] to understand their biological context. The list of UniProt accession numbers was uploaded and mapped against a reference *Danio rerio* dataset to extract and summarize molecular functions, biological processes, class of protein and clusters of functions. For protein–protein interaction network analysis, the BVA-analyzed differentially expressed proteins were subjected to STRING 10.0 (http://string-db.org)[32]. Interaction networks were obtained on the basis of confidence and evidence. The predicted associations between genes based on observed patterns of simultaneous expression were also considered.

2.11 Statistical analyses

All of our results are presented as mean± standard deviation (S.D.) in triplicate, at least. The gene expression levels and normalized values in all of the figures were compared using one-way ANOVA and Tukey's Multiple Comparison Test on Prism5 software (GraphPad, San Diego, USA). A probability value of

p<0.05 was considered significant.

3. Results

3.1 Trace metal accumulation and cytotoxicity of trace metals and TCDD

Studies of the biological mechanisms of trace metal toxicity reported in the existing literature have employed a wide dose range, perhaps reflecting the different sensitivities of different species and cell types. To keep a high percentage of cell viability, concentrations of 5%, 10%, and 25% LC50 values of Cu^{2+}, Zn^{2+}, Hg^{2+}, and As^{3+} were used to examine their effects on TCDD-induced reactions. As shown in Fig. 1, after 24 h exposure to increasing concentrations of these four trace metals alone or in the presence of 3 nM TCDD, Hg and As had accumulated in ZFL cells, and the accumulation was increased by TCDD, especially at high doses. Uptake of Cu and Zn by ZFL cells was not observed in our experiments. These findings suggest that ZFL cells can effectively eliminate essential metals, but the elimination mechanism is not effective for non-essential metals.

The combined cytotoxic effects of these four trace metals and TCDD (3/30nM) were determined using AlamarBlue™ assays. No significant toxic effects were observed in ZFL cells following the administration of metal ions and TCDD; the metal ions used in our experiments did not increase cell death induced by TCDD (Fig. 2).

3.2 Effects of trace metals and TCDD on EROD activity and cyp1a1

protein and mRNA expression

Trace metals were shown to differently regulate AHR target genes at the transcriptional and post-transcriptional level. To understand how these metals modulate the enzyme activity, protein and mRNA expression level of *cyp1a1*, ZFL cells were treated with different concentrations of Cu^{2+}, Zn^{2+}, Hg^{2+}, and As^{3+} alone and with 3 or 30 nM TCDD. None of the four metal ions had any significant effect on *cyp1a1* induction including enzyme activity (Fig. 3), protein (Fig. 4) and mRNA (Fig. 5) expression level. However, co-treatment with TCDD induced EROD enzyme activity (Fig. 3), and both protein levels (Fig. 4) and mRNA (Fig. 5) of *cyp1a1* were significantly decreased by Hg^{2+} and As^{3+}. Treatments with Cu^{2+} and Zn^{2+} had no effect on *cyp1a1* induction by TCDD. Similar regulations of these metals were observed on the mRNA expression level of *ahr2* and *arnt2b*, which are two upstream genes that mediate *cyp1a1* transcription. As the AHR2/ARNT2b complex plays an important role in CYP1A1 induction, decreased expression of these two genes could partially explain the reduction of CYP1A1 expression by Hg^{2+} and As^{3+}, perhaps due to the inhibition of transcriptional initiation.

3.3 Effects of trace metals on TCDD-Induced luciferase activity

To further examine whether the effect of trace metals on TCDD-mediated *cyp1a1* induction is regulated at the transcriptional initiation level, ZFL cells were transfected with TCDD-responsive CYP1A1 (P−2626/−2099) and 3XRE

constructs and then treated with 3 or 30 nM 2,3,7,8-TCDD in the absence or presence of Cu^{2+}, Zn^{2+}, Hg^{2+}, and As^{3+}at various concentrations. Compared to TCDD treatment alone, co-treatment with Hg^{2+} and As^{3+} reduced the magnitude of TCDD-induced luciferase activation in the 3XRE reporter. And for the CYP1A1 (P−2626/−2099) construct, although in some high concentration group (co-treatment with 30nM TCDD), the reduction in luciferase activity is not statistical significant, a decrease trend can be still observed (Fig. 6). Consistent with their regulation of CYP1A gene and protein expression levels, Cu^{2+} and Zn^{2+} had no effect on TCDD-induced luciferase activity. These results suggest that xenobiotic responsive elements not only conferred TCDD-responsiveness but also mediated the inhibition of Hg^{2+} and As^{3+} on TCDD-induced CYP1A1 gene transcription.

3.4 Differential expression of cytosolic proteins revealed by the proteomic approach

To further understand the response of AHR pathway inhibition by non-essential metals at the protein expression level, a proteomic approach was applied to reveal As^{3+}-induced differential protein expression after co-exposure with TCDD. Using 2-DE analyses, about 600 spots were detected in each image as shown in the representative image (Fig. 7). A total of 42 spots with different abundance were found in the As^{3+} and TCDD co-treatment group compared with the control and TCDD alone (Fig. 7). The locations of these 42

spots on a 2-D gel are marked and numbered (Fig.7 C) and amplified figures of each identified spot are shown in Fig. 8. Identified proteins with information and the average expression levels from three gels for each group are shown in Table 2. The density of those identified spots were also shown in Fig. S1 with significance after statistical analysis. Among these spots, 20 spots were up-regulated by TCDD treatment alone compared with the control group, 7 of them were further increased after co-treatment with As^{3+}, 12 were down-regulated, and the remaining one was not significantly affected by As^{3+} compared with the TCDD treatment group. Sixteen spots were down regulated by TCDD treatment alone, 3 were further diminished by As^{3+} co-treatment, 12 were further increased and 1 was not significantly affected. The 6 remaining spots were not significantly affected by TCDD; 5 of them increased after co-treatment and one decreased.

3.5 Bioinformatics analysis of identified proteins

To further explore cellular pathways and protein functions in response to As^{3+} and TCDD stress, the data obtained from the proteomic analysis were analyzed using PANTHER, DAVID and STRING. According to gene ontology analysis by PANTHER, the identified proteins were divided into 10 groups: chaperones, cytoskeletal proteins, glycolysis related enzymes, oxidoreductases, nucleic acid binding proteins, calcium-binding proteins, protein kinase activity, transporters, metal ion binding proteins and other

functions (Table 2). Exploring the annotations group by group rather than one by one, gene ontology enrichment analysis was performed by DAVID, which is a powerful tool grouping similar, redundant and homogeneous annotation content from the same or different sources into annotation groups[33, 34]. Similar annotation terms are grouped into clusters so that the user can read through the important terms block by block instead of individually. Using functional annotation clustering analysis in DAVID, the functions of 42 proteins were divided into 3 clusters focusing on glycolysis, nucleotide binding and ion binding (Table S1). The *p*-values of the first cluster (glycolysis) are all less than 0.05, which means the enrichment score is greater than 1.3, representing more important (enriched) terms. According to KEGG pathway analysis, the differential expressed proteins were mainly concentrated in glycolysis and gluconeogenesis, and fructose and mannose metabolism pathways.

As shown in Fig. 9, to find relevant proteins among the multiple identifications obtained by proteomic analysis, we subjected the list of the 42 different proteins from Table 2 to bioinformatics analysis in the STRING 10 database, which integrates interaction data from several bioinformatics sources and provides information about physical and functional properties, known and predicted interactions of genes and their products[35]. A general interaction network including all identified proteins is shown in Fig. 9A. DAVID was also used to highlight the functional annotation clustering inside the identified potential protein network. As shown in Fig. 9B, these proteins are

involved in metabolic processes, stress responses to chemical stimuli and oxidative processes according to the gene ontology descriptor “biological process.” According to their classification under the gene ontology descriptor “molecular function” the proteins are mainly for chemical binding and catalysis, as shown in Fig. 9C.

4. Discussion

Non-essential elements are toxic because they take over the binding sites of essential elements, and they are also usually persistent and thus have the potential to accumulate via the food chain, leading to human health problems if contaminated food is consumed. Essential elements such as Cu and Zn are needed for important metabolic functions[36], but can be toxic at higher concentrations, and excessive levels are damaging at the cellular level and to the organism as a whole[37]. The chemical basis of metal toxicology is still not sufficiently understood, but a uniform mechanism for all toxic metals is implausible due to great variation in chemical properties and toxicological endpoints[38]. The different effects of essential (Cu and Zn) and non-essential (As and Hg) metals on CYP1A1 induction observed in zebrafish further confirm the various and complicated toxic mechanisms involved in metal toxicity.

Although As and Hg are non-essential metals and do not have specific transport proteins or channels, they are transported via channels used by essential metals such as Cu and Zn. It has been reported that transport

proteins such as divalent metal transport 1 (DMT1) and Zn transporters (ZnT) can transport toxic metals from the intestine to internal organs such as the liver and cause toxicity if they are not removed quickly[40, 41]. However, essential metals are eliminated much more slowly than non-essential metals, resulting in the accumulation of essential metals, which can be significant if metal concentrations in the environment are beyond a certain threshold[42]. A study in Tilapia showed much higher accumulation of non-essential metals than essential metals, and the level of accumulated Cu was higher than Zn[42]. Similarly, the results of the present study demonstrate that the levels of Hg and As significantly increased in ZFL cells after exposure and a slightly increased level of Cu was also observed, whereas no accumulation of Zn was found, perhaps due to the high background level. These results suggest that the different effects of essential and non-essential metals on CYP1A1 induction might be due primarily to different levels of accumulated metals, and the metals that have high uptake and low elimination are expected to inhibit CYP1A1 induction.

CYP1A1 is the most widely studied Phase I CYP enzyme involved in PAH bio-activation in fish, and it is responsible for both metabolic activity and PAH detoxification[43]. Although several studies have reported that the induction of CYP1A1 in different species can be inhibited by metal treatments, the molecular response to CYP1A1 inhibition by trace metals was not investigated. Therefore, in this study, a proteomic approach was adopted to explore the

temporal changes in cytosolic protein expression that are associated with As^{3+} and TCDD intoxication in ZFL. Our results identified 42 proteins, which are mainly involved in metabolism, the stress response and oxidation.

Metabolic processes are known to play a vital role in determining the fates of environmental pollutants during biotic degradation. For instance, the expression level of several proteins is associated with glycolysis, and TCDD and As^{3+} affect gluconeogenesis. TCDD has been reported to disrupt glycolysis and gluconeogenesis by altering relevant enzyme activity[45]. Among these proteins, two classes of fructose-bisphosphate aldolases A/C-B (ALDO), enolase 1/3 (ENO) and L-lactate dehydrogenase (LDH) were down-regulated by TCDD, but co-exposure with As^{3+} up-regulated the expression levels of all of these proteins. Fructose bisphosphate aldolase takes part in the fourth step of glycolysis, catalyzing the cleavage of fructose 1,6-bisphosphate into glyceraldehyde3-phosphate[46]. Enolase is a key glycolytic enzyme that catalyzes the dehydration of 2-phosphoglycerate to phosphoenolpyruvate in the last step of the catabolic glycolytic pathway[47]. LDH catalyzes the last step in anaerobic glycolysis, the conversion of pyruvate to lactate, with the concomitant oxidation of NADH[48]. The down-regulation and up-regulation of glycolytic enzymes by TCDD/PAHs and trace metals, respectively, have been reported in previous studies[49-52], but their combined effects have not been reported. Because the glycolytic pathway is the major energy source for many cells, the effect of TCDD and As^{3+} on these proteins suggests that they might

both disturb energy metabolism.

Phosphoglycerate kinase (PGK), which catalyzes the reversible transfer of a phosphate group from 1,3-bisphosphoglycerate (1,3-BPG) to ADP producing 3-phosphoglycerate (3-PG) and ATP, was not affected by TCDD but increased by As^{3+} after co-treatment[53]. Triosephosphate isomerase B catalyzes the reversible interconversion of the triose phosphate isomers dihydroxyacetone phosphate and D-glyceraldehyde 3-phosphate[54]. Both these enzymes play a reversible role in catalysis and are involved in glycolysis and gluconeogenesis. The different effect of TCDD on these two enzymes compared to its effect on the glycolytic enzymes described above further supports the suggestion that TCDD might disrupt the glycolysis process, reducing energy production, and such inhibition could be reversed by As^{3+}. A similar disturbance of energy in response to AHR activation by PCBs has been reported[55]. Besides, increased expression of malate dehydrogenase (MDH), a mitochondrial enzyme involved in gluconeogenesis, following TCDD, but decreased after co-exposure with As^{3+} provided further evidence that TCDD might promote gluconeogenesis and As^{3+} might reverse the imbalance of energy metabolism caused by TCDD[56].

The second important pathway affected by TCDD and As^{3+} is the stress response to chemical insults. Chaperones constitute a large group of proteins associated with this process. For the six proteins with altered abundance, five heat shock proteins (HSPs) and one stress-induced phosphoprotein (STIP)

were identified in the proteomic studies. All of these proteins were down-regulated by TCDD alone, which is in line with the results of Sarioglu et al. (2006), which showed a marked down regulation of HSP90 in 5L rat hepatoma cells after treatment with TCDD[52]. Interestingly, after co-treatment with As^{3+}, all of these stress response proteins were up-regulated compared with TCDD exposure alone.

Induction of HSPs by trace metals is regarded as a defense mechanism in response to metal exposure[57, 58]. HSPs act as chaperones, which protect protein substrates from conformational damage and they can also act at multiple points in the apoptotic pathways to ensure that stress-induced damage does not inappropriately trigger cell death[59]. Stress-induced phosphoprotein is known as heat shock protein-organizing protein, and has a similar molecular function to the HSP family[60].. Before binding to TCDD, AHR has its own complex binding with many other proteins including HSP90, which is a chaperone that functions as a ligand binding AHR[61]. Although the HSP proteins identified in the current study are mainly from the HSP70 and 60 families, recent experimental results suggest that a number of co-chaperones, such as HSP70 and p60, are part of the HSP90-related multichaperone complex[62] and might associate with the AHR complex at various stages during the lifetime of the AHR[63, 64]. The main role of HSP90 in the AHR complex is to keep proper folding and stability of the AHR[65], and HSP70 appears to be important for protein folding involving HSP90[66]. Therefore, HSP70 might play

an important role in maintaining the stability of the AHR complex and the decreased abundance of these proteins indicates a reduced AHR complex level and thus increased AHR/ARNT2b heterodimers. Elevation of HSPs by As^{3+} suggests that more HSPs might be needed to form the AHR complex and keep it in the cytoplasm and to suppress the nuclear translocation of AHR to bind with ARNT.

Oxidative stress is also a response to toxicity. TCDD exerts many of its effects by inducing CYP1A1 gene expression, which increases electron transfer to molecular oxygen leading to the formation reactive oxygen species and lipid peroxidation[67]. Trace metals, including As^{3+}, have been reported to induce oxidative stress by cycling between oxidation states, or by interacting with antioxidants and increasing inflammation, resulting in the accumulation of free radicals in cells[68]. Therefore, a change in oxidation-related proteins would be expected with exposure to these metals.

The increased expression of glutathione reductase (GTR), which catalyzes the reduction of glutathione disulfide to the sulfhydryl form glutathione (GSH), and is a critical molecule in resisting oxidative stress and maintaining the reducing environment of the cell[69], might be viewed as a protective response to the oxidative stress induced by TCDD. However, the decreased expression level during co-exposure with As^{3+} suggests that As^{3+} might suppress this defense system. Increased GSH might cause the up-regulation of GTR and glutathione S-transferase P (GSTP1), a detoxification enzyme that catalyzes

the conjugation of many hydrophobic and electrophilic compounds with reduced GSH[70], which was also up-regulated by TCDD. This is in consistent with the findings that GSTP was also induced by TCDD in human hepatocyte cultures [71] and human breast cancer cells[72]. However, unlike GTR, As^{3+} further increased the level of GSTP after co-exposure. Both GTR and GSTP participate in the maintenance of cellular redox homeostasis through a number of convergent and divergent mechanisms; the relevant functional consequences associated with the opposite regulation of As^{3+} on these two proteins remains to be determined.

TCDD and As^{3+} treatment also changed the abundance of several structural proteins, including β-actin1 protein (ACTB), two tropomyosins (TPM4A, TPM3) and cofilin2 (CFL2). Tropomyosin, an important light chain regulatory protein in cardiac muscle, showed a small degree of up-regulation in the TCDD treated ZFL cells. This finding is consistent with several previous TCDD toxicological studies in which very similar pattern of up-regulations in various tropomyosin isoforms were observed[73, 74]. The levels of TPM binding protein and ACTB, another important globular multi-functional protein that forms microfilaments, were also increased by TCDD. As^{3+} further changed the abundance of these proteins after co-exposure. It appears likely that the alterations in their expression reflect an extensive reorganization of the cytoskeleton in ZFL cells.

We also observed changes in the abundance of numerous other proteins that had not yet shown to be affected by TCDD and As^{3+}, which may provide

novel starting points for the exploration of specific aspects of combined dioxin and metals toxicity. An example include the altered abundance of transketolase isoform X3, which has been reported to be involved in the reductive CBB cycle and non-oxidative part of the pentose phosphate pathway, and plays a critical role in connecting the pentose phosphate pathway to glycolytic intermediates[75]. Another interesting observation is the up-regulation of translationally controlled tumor protein homolog (TCTP), a growth-related, calcium binding and heat stable protein[76] with a crucial cellular role. Interestingly, recent reports describe human TCTP as a novel anti-apoptotic protein involved in cell survival[77, 78]. Up-regulation of this protein by TCDD and the further increase after co-treatment suggest that As may promote TCDD-induced cell proliferation. Further studies on this protein may yield interesting novel findings with regard to the combined toxicological mechanism of TCDD and trace metals.

In summary, differential regulation of the TCDD-induced AHR pathway by essential and non-essential metals was observed in ZFL cells. The uptake of the essential metals Cu and Zn was not significant in the cells and they had no impact on TCDD-induced toxicity or CYP1A1 levels. However, the non-essential metals As and Hg can be accumulated in ZFL cells, and thus inhibited the induction of CYP1A1 by TCDD through transcriptional initiation inhibition. Subsequently, a 2-DE proteomic approach was applied to study the changes of cytosolic proteins induced by TCDD and As^{3+} exposure. We

identified significant changes in the proteome of the ZFL cells following TCDD and As^{3+} exposure leading to alterations in metabolic processes, cellular stimulation responses and the cellular redox state of the ZFL cells. Collectively, the protein expression information provides insight into potential molecular mechanisms of TCDD and As^{3+} toxicity.

Conflict of interest statement

The authors declare that there are no conflicts of interest.

Acknowledgments

We thank the School of Life Sciences for its provision of a core facility and research allowance to conduct this research. Y. Y. Chen was the recipient of post-graduate studentships 2012-2015.

References

1. D. W. Nebert, A. Puga and V. Vasiliou, *Annals of the New York Academy of Sciences*, 1993, **685**, 624-640.
2. Z. Cao, J. Hong, R. E. Peterson and J. M. Aiken, *Aquat Toxicol*, 2000, **49**, 101-109.
3. D. I. Israel and J. P. Whitlock, Jr., *The Journal of biological chemistry*, 1983, **258**, 10390-10394.
4. G. Zeruth and R. S. Pollenz, *Chemico-biological interactions*, 2007, **170**, 100-113.
5. H. I. Swanson, *Chemico-biological interactions*, 2002, **141**, 63-76.
6. M. L. Scornaienchi, C. Thornton, K. L. Willett and J. Y. Wilson, *Arch Biochem Biophys*, 2010, **502**, 17-22.
7. M. E. Jonsson, D. G. Franks, B. R. Woodin, M. J. Jenny, R. A. Garrick, L. Behrendt, M. E. Hahn and J. J. Stegeman, *Chemico-biological interactions*, 2009, **181**, 447-454.
8. S. I. Karchner, D. G. Franks and M. E. Hahn, *The Biochemical journal*, 2005, **392**, 153-161.
9. R. L. Tanguay, C. C. Abnet, W. Heideman and R. E. Peterson, *Bba-Gene Struct Expr*, 1999, **1444**, 35-48.
10. E. A. Andreasen, M. E. Hahn, W. Heideman, R. E. Peterson and R. L. Tanguay, *Molecular*

pharmacology, 2002, **62**, 234-249.

11. M. E. Jonsson, M. J. Jenny, B. R. Woodin, M. E. Hahn and J. J. Stegeman, *Toxicological sciences : an official journal of the Society of Toxicology*, 2007, **100**, 180-193.
12. A. J. Hill, T. C. K. Heiden, W. Heideman and R. E. Peterson, *Zebrafish*, 2009, **6**, 79-91.
13. R. L. Tanguay, E. Andreasen, W. Heideman and R. E. Peterson, *Bba-Gene Struct Expr*, 2000, **1494**, 117-128.
14. V. P. Androutsopoulos, A. M. Tsatsakis and D. A. Spandidos, *BMC cancer*, 2009, **9**, 187.
15. D. C. Spink, B. H. Katz, M. M. Hussain, B. C. Spink, S. J. Wu, N. Liu, R. Pause and L. S. Kaminsky, *Drug Metab Dispos*, 2002, **30**, 262-269.
16. O. Barbier, G. Jacquillet, M. Tauc, M. Cougnon and P. Poujeol, *Nephron. Physiology*, 2005, **99**, p105-110.
17. L. Jarup, *British medical bulletin*, 2003, **68**, 167-182.
18. D. D. Vakharia, N. Liu, R. Pause, M. Fasco, E. Bessette, Q. Y. Zhang and L. S. Kaminsky, *Drug metabolism and disposition: the biological fate of chemicals*, 2001, **29**, 999-1006.
19. S. Kann, M. Y. Huang, C. Estes, J. F. Reichard, M. A. Sartor, Y. Xia and A. Puga, *Molecular pharmacology*, 2005, **68**, 336-346.
20. H. M. Korashy and A. O. El-Kadi, *Toxicology*, 2004, **201**, 153-172.
21. R. H. Elbekai and A. O. El-Kadi, *Toxicology*, 2004, **202**, 249-269.
22. A. Hill, C. V. Howard, U. Strahle and A. Cossins, *Toxicological sciences : an official journal of the Society of Toxicology*, 2003, **76**, 392-399.
23. J. Y. Zhu and K. M. Chan, *Metallomics : integrated biometal science*, 2012, **4**, 1064-1076.
24. Y. Y. Chen, J. Y. Zhu and K. M. Chan, *Aquat Toxicol*, 2014, **157**, 196-206.
25. B. A. Merrick, *Annals of the New York Academy of Sciences*, 2006, **1076**, 707-717.
26. W. K. Cheuk, P. C. Y. Chan and K. M. Chan, *Aquatic toxicology*, 2008, **89**, 103-112.
27. D. S. Chen, D. Q. Zhang, J. C. Yu and K. M. Chan, *Aquatic Toxicology*, 2011, **105**, 344-354.
28. C. J. Sinal and J. R. Bend, *Molecular pharmacology*, 1997, **52**, 590-599.
29. D. S. Chen and K. M. Chan, *Aquatic toxicology*, 2011, **104**, 270-277.
30. H. Y. Mi and P. Thomas, *Methods Mol Biol*, 2009, **563**, 123-140.
31. D. W. Huang, B. T. Sherman and R. A. Lempicki, *Nucleic acids research*, 2009, **37**, 1-13.
32. D. Szklarczyk, A. Franceschini, M. Kuhn, M. Simonovic, A. Roth, P. Minguez, T. Doerks, M. Stark, J. Muller, P. Bork, L. J. Jensen and C. von Mering, *Nucleic acids research*, 2011, **39**, D561-568.
33. H. Tipney and L. Hunter, *Human genomics*, 2010, **4**, 202-206.
34. D. W. Huang, B. T. Sherman and R. A. Lempicki, *Nat Protoc*, 2009, **4**, 44-57.
35. A. Franceschini, D. Szklarczyk, S. Frankild, M. Kuhn, M. Simonovic, A. Roth, J. Lin, P. Minguez, P. Bork, C. von Mering and L. J. Jensen, *Nucleic acids research*, 2013, **41**, D808-815.
36. J. F. Provencher, B. M. Braune, H. G. Gilchrist, M. R. Forbes and M. L. Mallory, *Sci Total Environ*, 2014, **476**, 308-316.
37. R. Singh, N. Gautam, A. Mishra and R. Gupta, *Indian J Pharmacol*, 2011, **43**, 246-253.
38. A. Serafim, R. Company, B. Lopes, J. Rosa, A. Cavaco, G. Castela, E. Castela, N. Olea and M. J. Bebianno, *Journal of toxicology and environmental health. Part A*, 2012, **75**, 867-877.
39. M. Eide, M. Rusten, R. Male, K. H. M. Jensen and A. Goksoyr, *Aquatic toxicology*, 2014, **147**, 7-17.
40. S. J. Cobbina, Y. Chen, Z. Zhou, X. Wu, W. Feng, W. Wang, G. Mao, H. Xu, Z. Zhang and L. Yang, *Chemosphere*, 2015, **132**, 79-86.

41. D. A. Vesey, *Toxicol Lett*, 2010, **198**, 13-19.
42. T. Ichise, M. Kano, K. Hashimoto, D. Yanagihara, K. Nakao, R. Shigemoto, M. Katsuki and A. Aiba, *Science*, 2000, **288**, 1832-1835.
43. D. W. Nebert, T. P. Dalton, A. B. Okey and F. J. Gonzalez, *The Journal of biological chemistry*, 2004, **279**, 23847-23850.
44. J. Klose, C. Nock, M. Herrmann, K. Stuhler, K. Marcus, M. Bluggel, E. Krause, L. C. Schalkwyk, S. Rastan, S. D. Brown, K. Bussow, H. Himmelbauer and H. Lehrach, *Nature genetics*, 2002, **30**, 385-393.
45. C. Lu, Y. Wang, Z. Sheng, G. Liu, Z. Fu, J. Zhao, X. Yan, B. Zhu and S. Peng, *Toxicol Appl Pharmacol*, 2010, **248**, 178-184.
46. L. Macomber, S. P. Elsey and R. P. Hausinger, *Mol Microbiol*, 2011, **82**, 1291-1300.
47. A. Diaz-Ramos, A. Roig-Borrellas, A. Garcia-Melero and R. Lopez-Alemany, *Journal of biomedicine & biotechnology*, 2012, **2012**, 156795.
48. G. Auerbach, R. Ostendorp, L. Prade, I. Korndorfer, T. Dams, R. Huber and R. Jaenicke, *Struct Fold Des*, 1998, **6**, 769-781.
49. A. Oberemm, C. Meckert, L. Brandenburger, A. Herzig, Y. Lindner, K. Kalenberg, E. Krause, C. Ittrich, A. Kopp-Schneider, R. Stahlmann, H. B. Richter-Reichhelm and U. Gundert-Remy, *Toxicology*, 2005, **206**, 33-48.
50. S. H. G. Maureen A Soh, Seema Somji, Jane R Dunlevy, Xu Dong Zhou, Mary Ann Sens, Chandra S Bathula, Christina Allen and Donald A Sens, *Cancer Cell International 2011,*, 2011, **11**, 41-53.
51. V. Carriere, A. Rodolosse, M. Lacasa, D. Cambier, A. Zweibaum and M. Rousset, *The American journal of physiology*, 1998, **274**, G1101-1108.
52. H. Sarioglu, S. Brandner, C. Jacobsen, T. Meindl, A. Schmidt, J. Kellermann, F. Lottspeich and U. Andrae, *Proteomics*, 2006, **6**, 2407-2421.
53. A. Dhar, A. Samiotakis, S. Ebbinghaus, L. Nienhaus, D. Homouz, M. Gruebele and M. S. Cheung, *Proceedings of the National Academy of Sciences of the United States of America*, 2010, **107**, 17586-17591.
54. J. L. Seigle, A. M. Celotto and M. J. Palladino, *Genetics*, 2008, **179**, 855-862.
55. W. Zhang, R. M. Sargis, P. A. Volden, C. M. Carmean, X. J. Sun and M. J. Brady, *PloS one*, 2012, **7**, e37103.
56. R. A. Musrati, M. Kollarova, N. Mernik and D. Mikulasova, *General physiology and biophysics*, 1998, **17**, 193-210.
57. T. Kusakabe, K. Nakajima, K. Nakazato, K. Suzuki, H. Takada, T. Satoh, M. Oikawa, K. Arakawa and T. Nagamine, *Toxicol in Vitro*, 2008, **22**, 1469-1475.
58. S. G. Han, V. Castranova and V. Vallyathan, *Mol Cell Biochem*, 2005, **277**, 153-164.
59. E. Schmitt, M. Gehrmann, M. Brunet, G. Multhoff and C. Garrido, *J Leukocyte Biol*, 2007, **81**, 15-27.
60. T. H. Wang, A. Chao, C. L. Tsai, C. L. Chang, S. H. Chen, Y. S. Lee, J. K. Chen, Y. J. Lin, P. Y. Chang, C. J. Wang, A. S. Chao, S. D. Chang, T. C. Chang, C. H. Lai and H. S. Wang, *Mol Cell Proteomics*, 2010, **9**, 1873-1884.
61. P. K. Mandal, *Journal of comparative physiology. B, Biochemical, systemic, and environmental physiology*, 2005, **175**, 221-230.
62. K. D. Dittmar, K. A. Hutchison, J. K. Owens-Grillo and W. B. Pratt, *The Journal of biological*

chemistry, 1996, **271**, 12833-12839.

63. S. C. Nair, E. J. Toran, R. A. Rimerman, S. Hjermstad, T. E. Smithgall and D. F. Smith, *Cell stress & chaperones*, 1996, **1**, 237-250.
64. J. R. Petrulis and G. H. Perdew, *Chemico-biological interactions*, 2002, **141**, 25-40.
65. J. McGuire, M. L. Whitelaw, I. Pongratz, J. A. Gustafsson and L. Poellinger, *Molecular and cellular biology*, 1994, **14**, 2438-2446.
66. P. Csermely, T. Schnaider, C. Soti, Z. Prohaszka and G. Nardai, *Pharmacology & therapeutics*, 1998, **79**, 129-168.
67. E. A. Hassoun, F. Li, A. Abushaban and S. J. Stohs, *Journal of applied toxicology : JAT*, 2001, **21**, 211-219.
68. S. J. S. Flora, *Free Radical Bio Med*, 2011, **51**, 257-281.
69. H. J. Cohen, E. H. Tape, J. Novak, M. E. Chovaniec, P. Liegey and J. C. Whitin, *Blood*, 1987, **69**, 493-500.
70. R. N. Armstrong, *Chemical research in toxicology*, 1991, **4**, 131-140.
71. D. Schrenk, T. Stuven, G. Gohl, R. Viebahn and K. W. Bock, *Carcinogenesis*, 1995, **16**, 943-946.
72. D. Hoivik, C. Wilson, W. L. Wang, K. Willett, R. Barhoumi, R. Burghardt and S. Safe, *Arch Biochem Biophys*, 1997, **348**, 174-182.
73. J. Zhang, K. A. Lanham, W. Heideman, R. E. Peterson and L. Li, *Journal of proteome research*, 2013, **12**, 3093-3103.
74. R. Ishimura, S. Ohsako, T. Kawakami, M. Sakaue, Y. Aoki and C. Tohyama, *Toxicol Appl Pharmacol*, 2002, **185**, 197-206.
75. C. W. Hu, Y. L. Chang, S. J. Chen, L. L. Kuo-Huang, J. C. Liao, H. C. Huang and H. F. Juan, *PloS one*, 2011, **6**.
76. P. Bangrak, P. Graidist, W. Chotigeat and A. Phongdara, *J Biotechnol*, 2004, **108**, 219-226.
77. F. Li, D. Zhang and K. Fujise, *Journal of Biological Chemistry*, 2001, **276**, 47542-47549.
78. D. Zhang, F. Li, D. Weidner, Z. H. Mnjoyan and K. Fujise, *Journal of Biological Chemistry*, 2002, **277**, 37430-37438.

Figure legends

Fig. 1 Metal levels in ZFL cells. ZFL cells were exposed to 5%, 10%, or 25% LC50 of Cu^{2+}, Zn^{2+}, Hg^{2+}, and As^{3+} alone or in the presence of 3 nM TCDD for 24 h. After exposure, ZFL cells were collected and digested for uptake measurements. Values are means ± S.D. Tukey's multiple comparison test was used to compare the accumulation level from different treatments in each group (same letter indicates no significant difference).

Fig. 2 Combined cytotoxicities of As^{3+}, Cu^{2+}, Hg^{2+}, Zn^{2+} and TCDD on ZFL cells. ZFL cells were exposed to different concentrations of Cu^{2+}, Zn^{2+}, Hg^{2+}, As^{3+} and TCDD for 24 h. The data are expressed as percentage of untreated control, which is set at 100%, ±S.D. (N = 6).

Fig. 3 Effects of As^{3+}, Cu^{2+}, Hg^{2+} and Zn^{2+} on the induction of EROD activity in ZFL cells. Cells were treated with 5%, 10%, or 25% LC50 of Cu^{2+}, Zn^{2+}, Hg^{2+}, and As^{3+} alone or in the presence of 3 nM TCDD for 24 h. The values represent mean activity ± S.D. (N = 6). The data were analyzed by one-way ANOVA (*p < 0.01, **p < 0.05, ***p < 0.005) comparing each group with the control. Tukey's multiple comparison test was used to compare results of fold inductions from different treatments in each group (same letter indicates no significant difference).

Fig. 4 Effect of As^{3+}, Cu^{2+}, $Hg^{2+}$and Zn^{2+} on TCDD-induced CYP1A1 protein. ZFL cells were treated for 24 h with increasing concentrations of Cu^{2+}, Zn^{2+}, Hg^{2+}, and As^{3+} alone or in the presence of 3 nM TCDD. The intensity of CYP1A1 protein bands was normalized to GAPDH signals, which were used as a loading control. One of three representative experiments is shown.

Fig. 5 Effects of As^{3+} (A), Cu^{2+} (B), Hg^{2+} (C), Zn^{2+} (D) and TCDD on the mRNA expression level of *cyp1a1*, *ahr2* and *arnt2b* in ZFL cells after a 24-h treatment. The results are represented as the mean± S.D. of six replicates. The data were analyzed by one-way ANOVA (*p < 0.01, **p < 0.05, ***p < 0.005), comparing each group with the control. Tukey's multiple comparison test was used to compare the results of fold inductions from different group.

Fig. 6 Dual luciferase assay of TCDD-inducible gene constructs (P-2626/-2099 and 3XRE) in ZFL cells exposed to As^{3+}, Cu^{2+}, Hg^{2+}, Zn^{2+} and TCDD. The transfected cells were treated with TCDD alone or in the presence of As^{3+}, Cu^{2+}, $Hg^{2+}$and Zn^{2+} for 24 h. The bars represent the mean ±S.D. of the three replicates. (p < 0.05, n = 3, one-way ANOVA, Tukey's test).

Fig. 7 Representative image of CBB stained 2-DE gel (A: Control; B TCDD; C: TCDD + AS^{3+}). Total cytosolic proteins were loaded and separated using

IPG strips (pH 3–10)/SDS-PAGE (10% acrylamide). The circled spots represent the matched spots in the three gels, and the spot numbers refer to the proteins with modified abundance after TCDD and AS^{3+} treatment that were selected for mass spectrometry (see Table2).

Fig. 8 Magnified images of protein spots that showed significantly different changes. Zoom-in regions of typical 2-DE demonstrate the effect of TCDD and joint TCDD and AS^{3+} exposure on the regulation of these identified proteins. The protein name of each spot is shown in Table 1.

Fig. 9 Protein–protein interaction network visualized on the STRING website. The list of identified proteins was subjected to STRING (v. 10) analysis to reveal functional interactions between the proteins which expression level were affected either by TCDD treatment alone or TCDD and As^{3+} co-treatment. Each node represents a protein, and each edge represents an interaction. The original graphic output was modified to fit the proteins, according to their classification under the gene ontology descriptors “biological process” (B): metabolic process (confined within the black circle), response to chemical stimulus (confined within the red circle) and oxidative process (confined within the blue circle), and “molecular function” (C): catalytic and binding (confined within the black and red circle respectively) as revealed by the Database for Annotation (DAVID)

Fig. S1 Protein abundance of identified protein spots. The values represent mean density ± S.D. (N = 3). The data were analyzed by one-way ANOVA (*$p < 0.01$, **$p < 0.05$, ***$p < 0.005$) comparing each group with the control. Tukey’s multiple comparison test was used to compare results of fold inductions from different treatments in each group (same letter indicates no significant difference).

Table 1 Nucleotide sequences of primers in the gene expression analysis using real-time quantitative PCR assay.

Gene (Accession number)	Primer	Nucleotide Sequence (5′–3′)
gapdh (NM_213094)	Forward	CGACCTCACCTGCCGCCTTACA
	Reverse	GTCATTGAGGGAGATGCCAGCG
cyp1a1 (AF210727.2)	Forward	CGCTTGTATGGGCTTGTCCT
	Reverse	CGCAGCTAAAACAGGCACTC
ahr2 (NM_131264.1)	Forward	ACGGTGAAGCTCTCCCATA
	Reverse	AGTAGGTTTCTCTGGCCAC
arnt2b (AY007992.1)	Forward	CCGCTGTAAACCCATCGGAA
	Reverse	AATCCATCCCCGCTGATCTC

Table 2. Identified proteins differentially expressed in the ZFL cells after As^{3+} and TCDD treatment.

Spot No.	Protein Name	Accession No.	Gene Symbol	MW (kDa)/Pi	Individual spot intensity/total intensity (average value %)		
					Control	TCDD	TCDD+ As^{3+}
Chaperones							
2	heat shock protein 5	gi|39645428	hspa5	71.90/5.04	0.082	0.0134	0.212
3	heat shock cognate 71 kDa protein	gi|160333682	hsp70l	71.10/5.31	0.118	0.109	0.302
4	heat shock cognate 70-kd protein	gi|18858871	hsp70l	72.40/6.29	0	0	0.112
5	heat shock 70 kDa protein	gi|528474057	hsp70	70.40/5.53	0	0	0.0184
6	stress-induced-phosphoprotein 1	gi|56090148	stip1	61.60/6.43	0.0298	0.0215	0.0594
8	60 kDa heat shock protein	gi|31044489	hspd1	61.20/5.56	0.0753	0.0674	0.1148
Cytoskeletal proteins							
17	Bactin1 protein	gi|28279111	actb1	41.70/5.3	0.0887	0.153	0.112
29	tropomyosin alpha-4 chain isoform 2	gi|47085929	tpm4a	28.50/4.63	0.110	0.155	0.208
30	tropomyosin alpha-3 chain isoform 2	gi|41393141	tpm3	28.80/4.76	0.0148	0.038	0.0588
42	cofilin 2	gi|47271384	cfl2	18.80/6.84	0.0248	0.0153	0.0128
Glycolysis-related enzymes							
13	alpha-enolase	gi|47085883	enoa	47.00/6.16	0.0162	0.0099	0.0285
15	enolase 3, (beta, muscle)	gi|68086449	eno3	47.40/6.19	0.0397	0.0318	0.0694
21	Pgk1 protein	gi|41388972	pgk1	44.70/6.47	0.0343	0.035	0.0678
20	fructose-bisphosphate aldolase	gi|35902900	aldocb	39.20/6.21	0.0217	0.0191	0.0453

	C-B						
22	fructose-bisphosphate aldolase A	gi|41282154	aldoa	39.70/8.45	0.0913	0.0614	0.0326
26	L-lactate dehydrogenase B-A chain	gi|18858961	ldhba	36.20/6.39	0.0236	0.022	0.0414
39	triosephosphate isomerase B	gi|47271422	tpi1b	26.80/6.9	0.0709	0.142	0.0614
Oxidoreductases							
9	prolyl 4-hydroxylase subunit alpha-2 precursor X1	gi|55925444	p4ha2	58.80/5.46	0.0145	0.0088	0.02
16	PREDICTED: glutathione reductase, mitochondrial isoform X2	gi|528500417	gsr	50.70/6.92	0.076	0.123	0.086
19	4-hydroxyphenyl pyruvate dioxygenase	gi|51230599	hpd	44.60/5.84	0.0254	0.0125	0.0117
31	electron transfer flavoprotein subunit alpha, mitochondrial	gi|38707985	etfa	35.10/6.91	0.0178	0.0087	0.0101
32	malate dehydrogenase, mitochondrial	gi|47085883	mdh	35.40/8.4	0.024	0.0231	0.0167
40	glutathione S-transferase pi	gi|18858197	gstp1	23.50/8.17	0.00562	0.0112	0.032
41	flavin reductase	gi|50540440	fre	21.10/8.72	0.00869	0.0133	0.0282
Nucleic acid binding proteins							
1	CDC48	gi|34740143	CDC48	89.40/5.13	0.0661	0.0233	0.0202
11	UV excision repair protein RAD23 homolog B isoform X1	gi|528512712	RAD23B	40.00/4.62	0.0198	0.0278	0.0268
14	Sjogren syndrome antigen B (autoantigen La)	gi|41054695	ssb	46.10/6.68	0.0568	0.0613	0.0345
18	PREDICTED:	gi|52849	hnrnpab	36.10/5.2	0.0238	0.016	0.0101

	heterogeneous nuclear ribonucleoprotein A/B isoform X1	9299					
27	heterogeneous nuclear ribonucleoprotein A/B	gi|47086935	HNRNPAB	34.20/6.85	0.112	0.145	0.117
33	elongation factor 1-beta isoform X2	gi|528481866	eef1b2	15.60/4.16	0.0747	0.0789	0.142
Calcium-binding proteins							
10	calreticulin 3b precursor	gi|50355968	calr3b	48.30/4.34	0.0569	0.0598	0.152
24	Annexin A1a	gi|31419751	anxa1a	37.70/5.93	0.142	0.167	0.113
28	Annexin A2a	gi|38566042	anxa2a	38.10/7.56	0.122	0.178	0.118
37	translationally-controlled tumor protein homolog	gi|37700237	tpt1	19.00/4.52	0.126	0.115	0.226
Protein kinase activity-related proteins							
25	Si:dkey-180p18.9 protein	gi|63101286	Si:dkey-180p18.9	38.90/6.55	0.0453	0.0520	0.0589
34	adenylate kinase 2, mitochondrial isoform X1	gi|528510213	ak2	25.80/5.53	0.0256	0.0141	0.0165
Transporters							
23	inorganic pyrophosphatase	gi|62955639	ppa	32.60/5.25	0.0636	0.0587	0.102
Metal ion binding proteins							
7	transketolase isoform X3	gi|528517580	Tkt	63.00/7.21	0.148	0.311	0.223
Others							
12	uncharacterized protein LOC405841 precursor	gi|47086229	LOC405841	54.60/4.92	0.0198	0.0278	0.0372
35	proteasome subunit alpha type-1	gi|51010945	psma1	29.20/6.20	0.0228	0.0202	0.0493
36	bisphosphoglyce	gi|38488	pgam1a	28.90/6.1	0.0130	0.0169	0.0134

	rate mutase 1a	700		9			
38	uncharacterized protein LOC100145226	gi|187608635	LOC100145226	22.30/6.08	0.0289	0.0183	0.0176

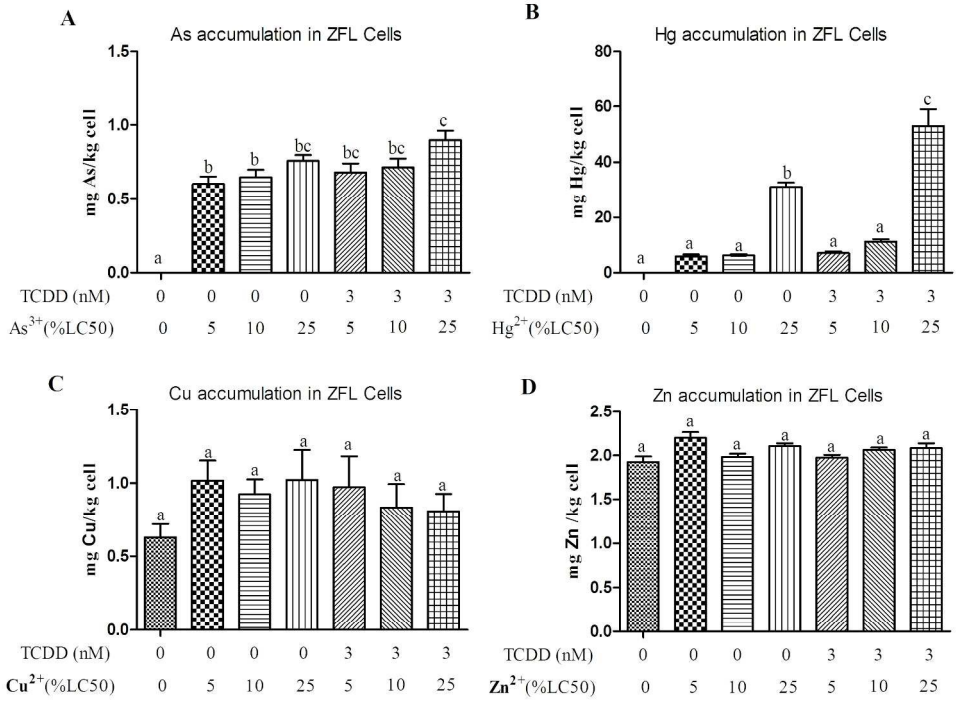

248x184mm (300 x 300 DPI)

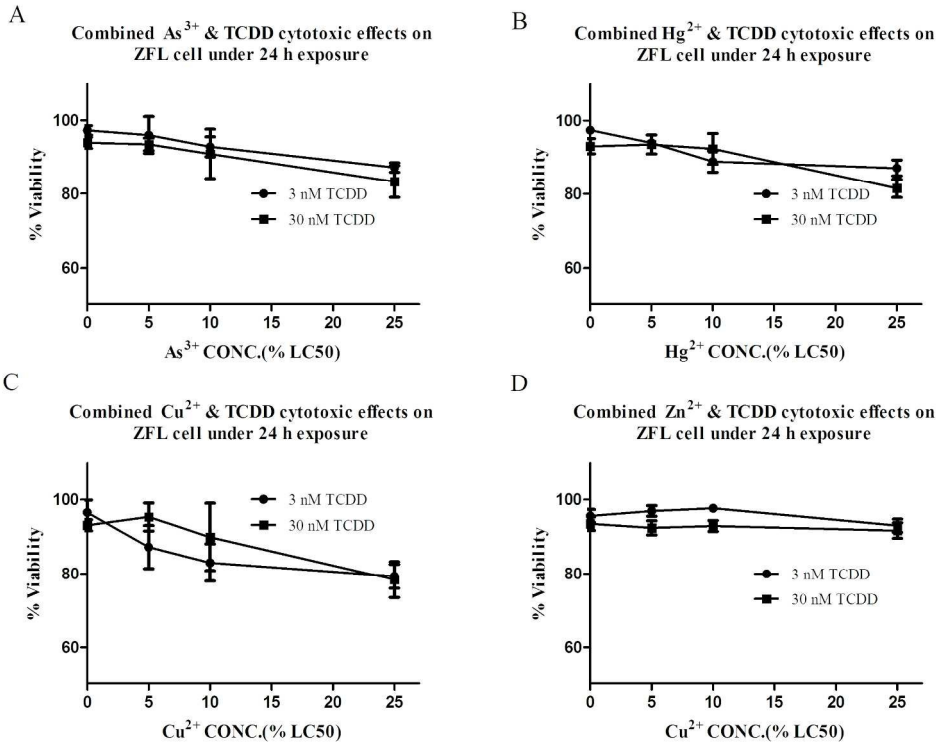

228x180mm (300 x 300 DPI)

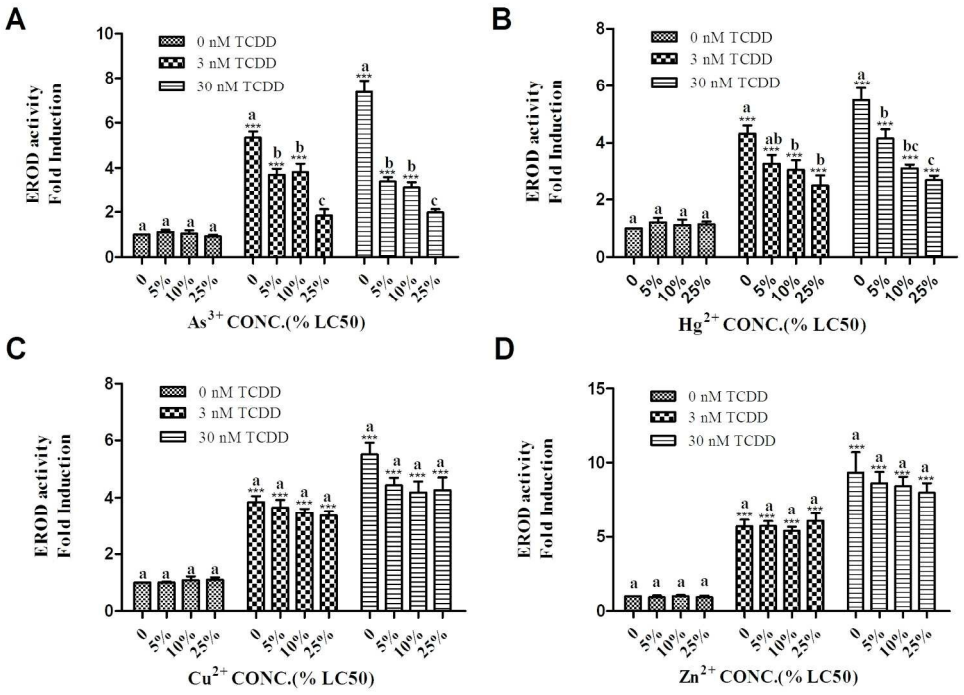

184x138mm (300 x 300 DPI)

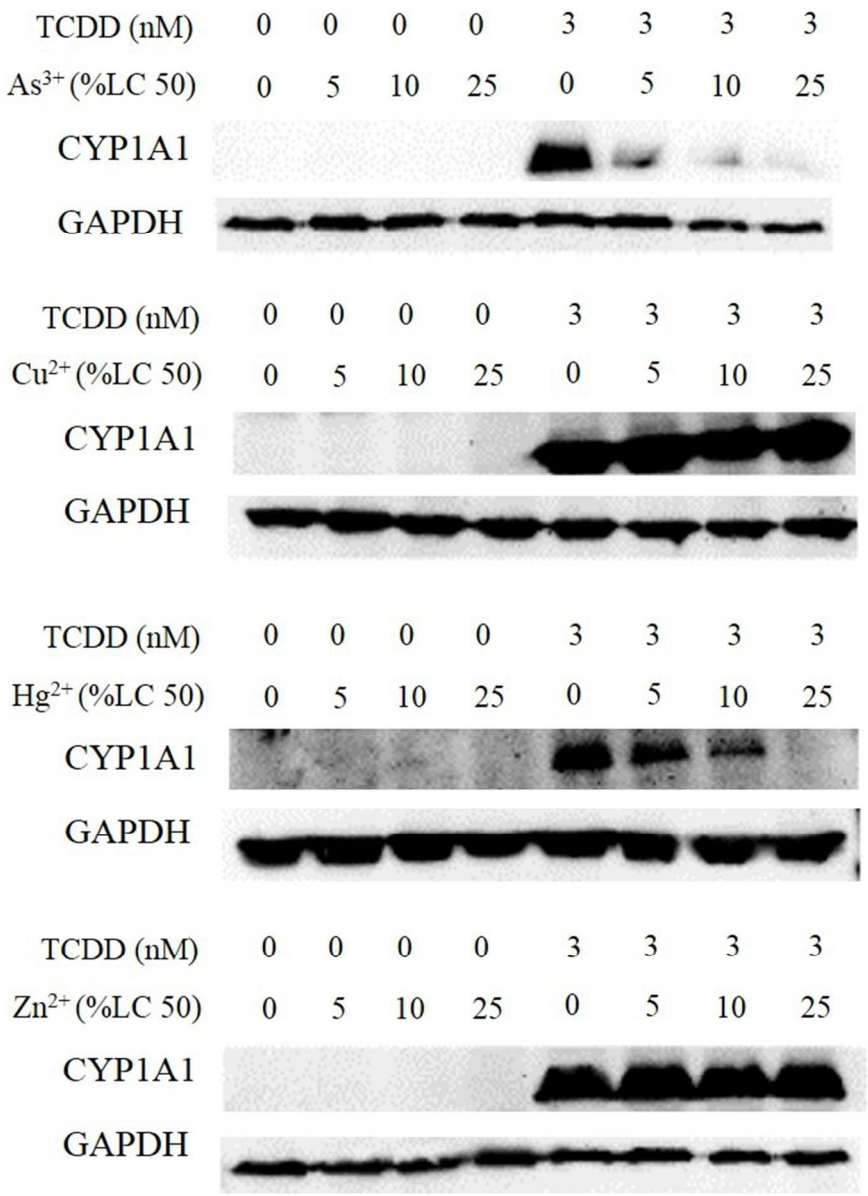

119x161mm (150 x 150 DPI)

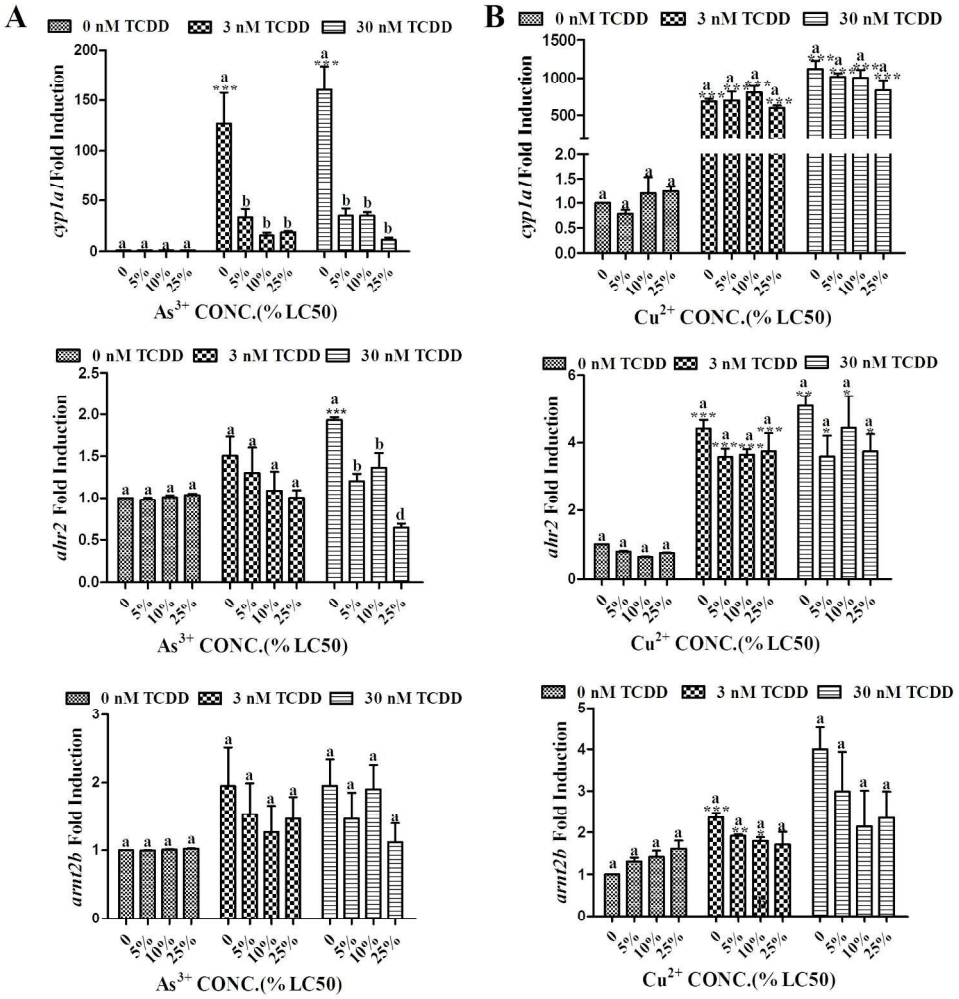

195x204mm (300 x 300 DPI)

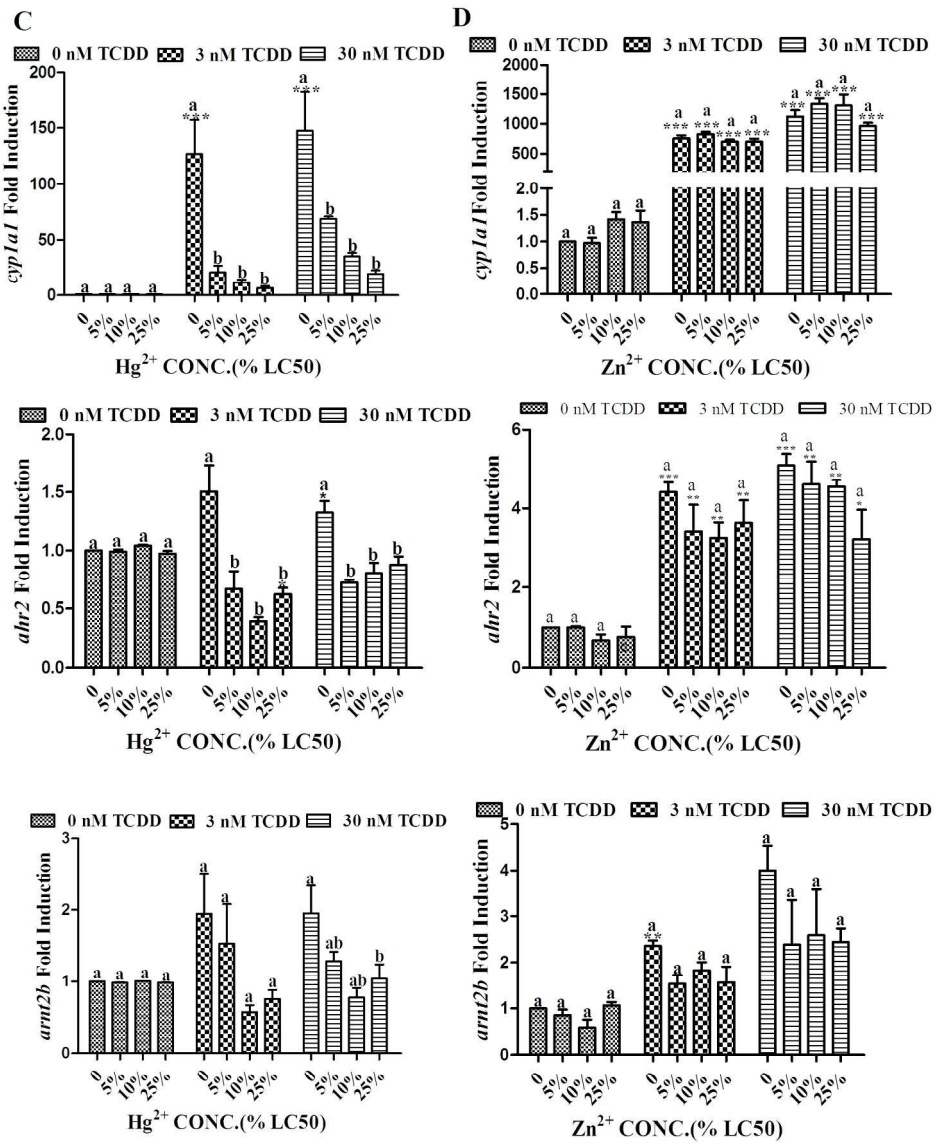

206x245mm (300 x 300 DPI)

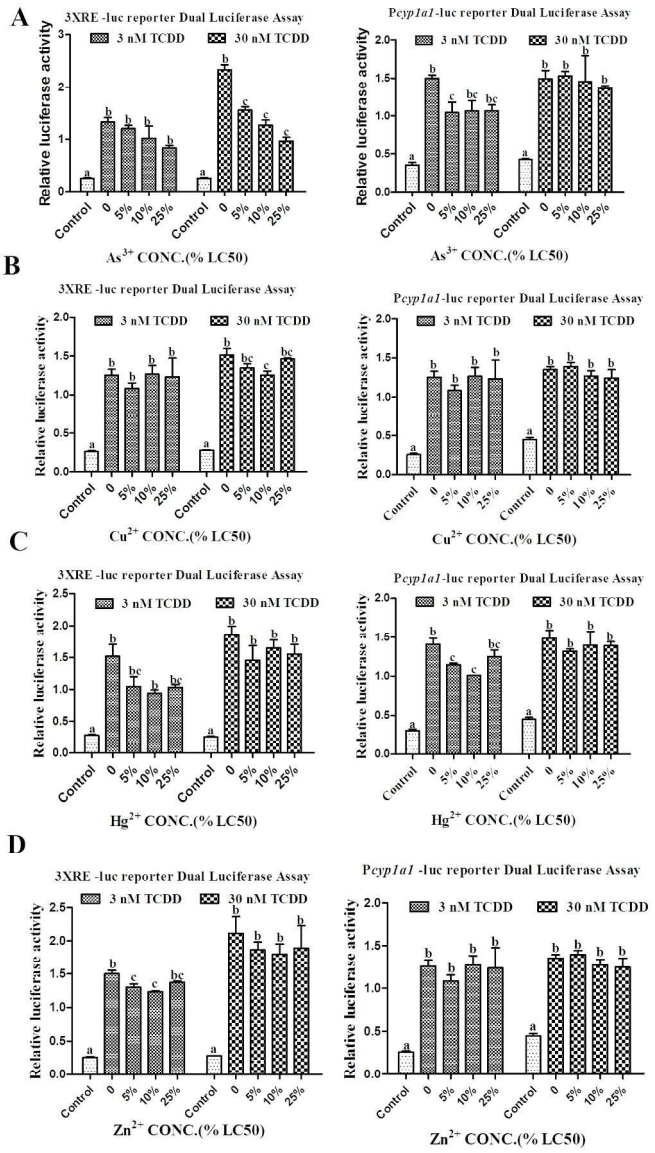

200x247mm (300 x 300 DPI)

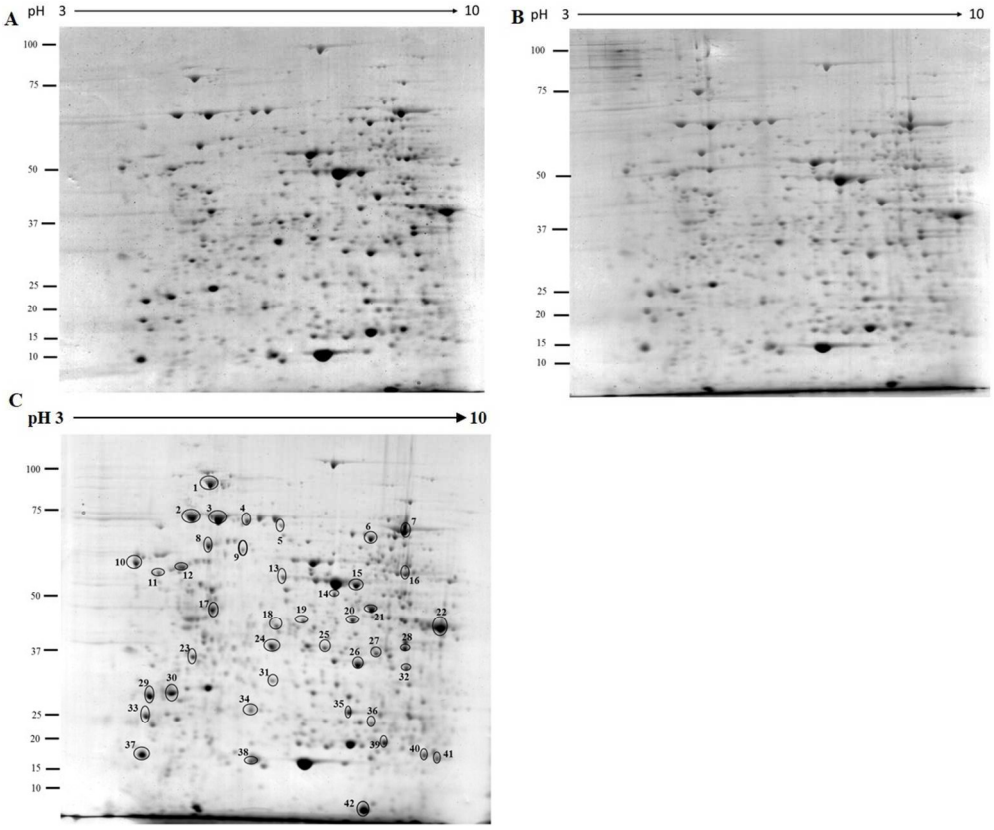

203x168mm (150 x 150 DPI)

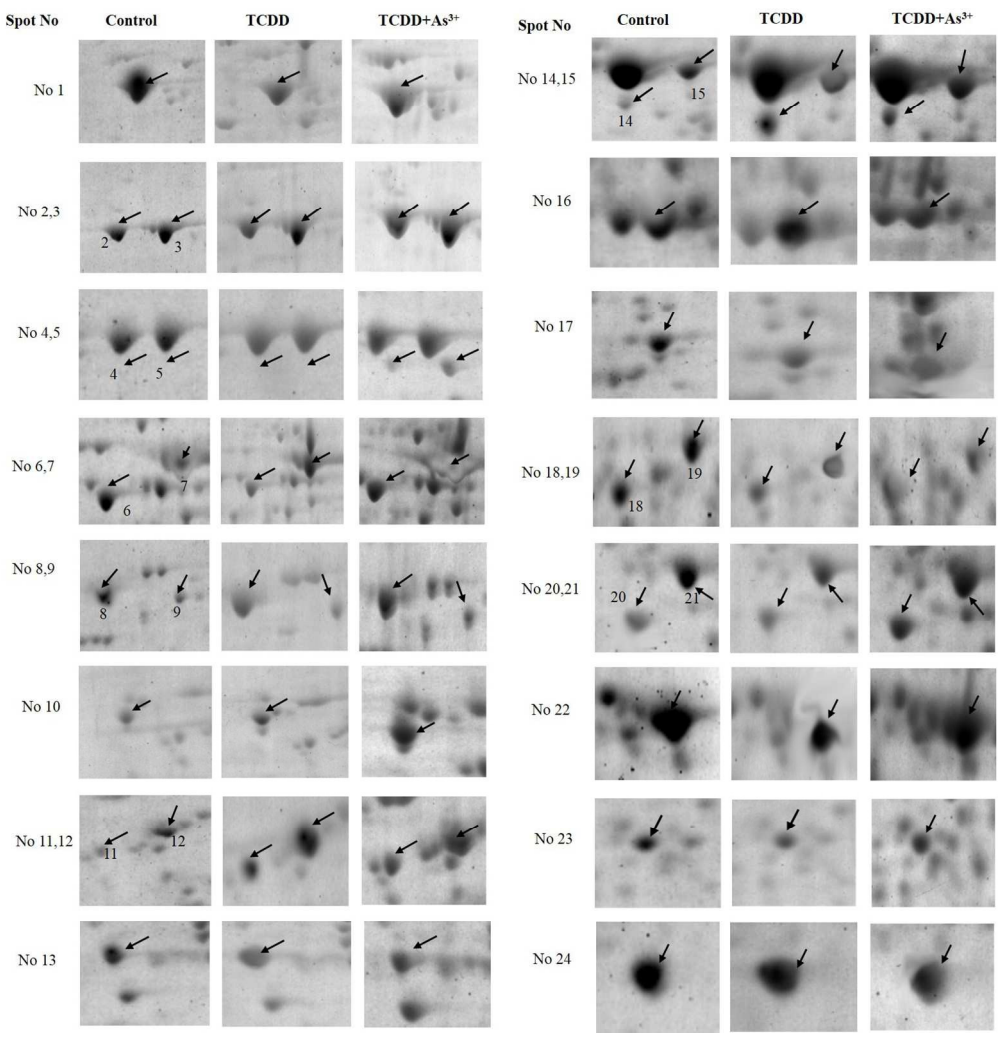

272x279mm (150 x 150 DPI)

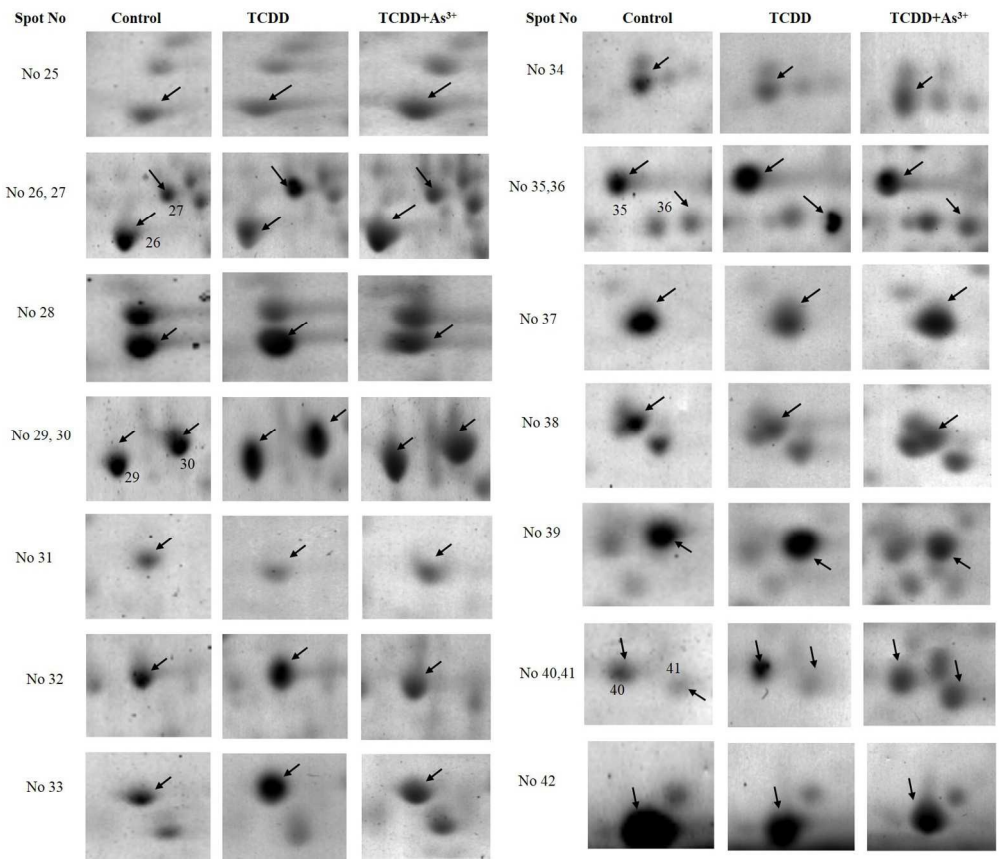

281x240mm (150 x 150 DPI)

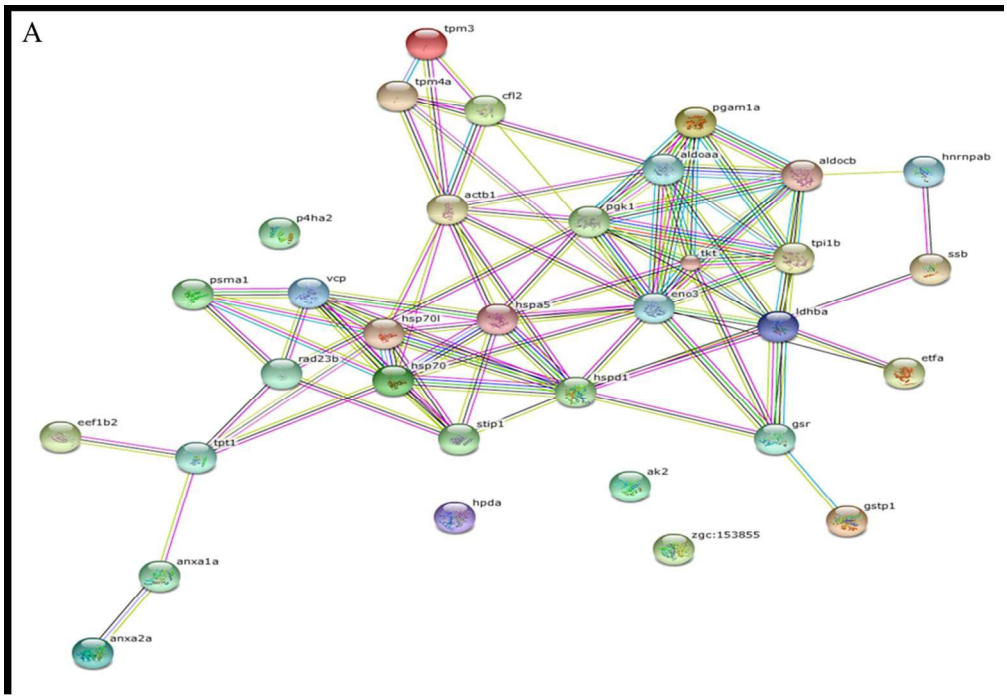

245x168mm (150 x 150 DPI)

B

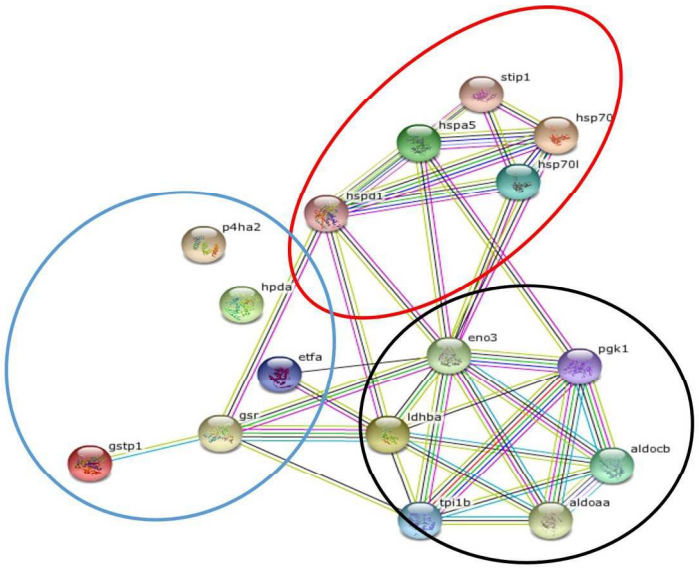

314x176mm (150 x 150 DPI)

C

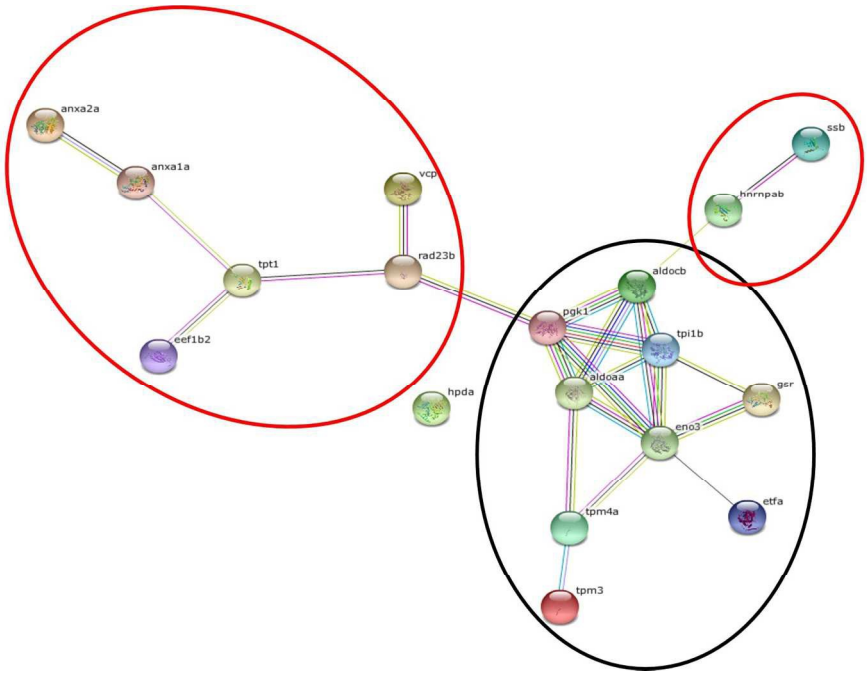

288x191mm (150 x 150 DPI)